Photoluminescence of Eu^{3+}-, Tb^{3+}-, Dy^{3+}- and Tm^{3+}-doped transparent GeO_2–TiO_2–K_2O glass ceramics

2008 J. Phys.: Condens. Matter 20 335106

(http://iopscience.iop.org/0953-8984/20/33/335106)

J. Phys.: Condens. Matter **20** (2008) 335106 (11pp) doi:10.1088/0953-8984/20/33/335106

Photoluminescence of Eu^{3+}-, Tb^{3+}-, Dy^{3+}- and Tm^{3+}-doped transparent GeO_2–TiO_2–K_2O glass ceramics

G Lakshminarayana[1,4], Jianrong Qiu[1], M G Brik[2] and I V Kityk[3]

[1] State Key Laboratory of Silicon Materials, Zhejiang University, Hangzhou 310027, People's Republic of China
[2] Institute of Physics, University of Tartu, Riia 142, Tartu 51014, Estonia
[3] Department of Chemistry, Silesian University of Technology, ulica Marcina Strzody 9, PL-44100 Gliwice, Poland

E-mail: glnphysics@rediffmail.com

Received 11 June 2008
Published 28 July 2008
Online at stacks.iop.org/JPhysCM/20/335106

Abstract

In this paper, we present the photoluminescence properties of Eu^{3+}-, Tb^{3+}-, Dy^{3+}- and Tm^{3+}-doped potassium–titanium–germanate glasses and glass ceramics. Following the x-ray diffraction measurement, the glass structure was established. Compared to Eu^{3+}-, Tb^{3+}-, Dy^{3+}- and Tm^{3+}-doped glasses, their respective glass ceramics show stronger emissions due to the presence of the $K_2TiGe_3O_9$ crystalline phase. For Eu^{3+}-doped glass and glass ceramics, five emission bands centered at 578 nm ($^5D_0 \rightarrow {}^7F_0$), 592 nm ($^5D_0 \rightarrow {}^7F_1$), 614 nm ($^5D_0 \rightarrow {}^7F_2$), 653 nm ($^5D_0 \rightarrow {}^7F_3$) and 702 nm ($^5D_0 \rightarrow {}^7F_4$) have been observed with 394 nm ($^5D_0 \rightarrow {}^7L_6$) excitation wavelength. Of them, 614 nm ($^5D_0 \rightarrow {}^7F_2$) has shown a bright reddish-orange emission. For Tb^{3+}-doped glass and glass ceramic, four emission bands centered at 490 nm ($^5D_4 \rightarrow {}^7F_6$), 549 nm ($^5D_4 \rightarrow {}^7F_5$), 586 nm ($^5D_4 \rightarrow {}^7F_4$) and 621 nm ($^5D_4 \rightarrow {}^7F_3$) have been observed with an excitation at 378 nm ($^3F_6 \rightarrow {}^5G_6$) wavelength. Of them, 549 nm ($^5D_4 \rightarrow {}^7F_5$) has shown a bright green emission. With regard to Dy^{3+}:glass and glass ceramic, a blue emission band centered at 485 nm ($^4F_{9/2} \rightarrow {}^6H_{15/2}$) and a bright fluorescent yellow emission at 576 nm ($^4F_{9/2} \rightarrow {}^6H_{13/2}$) have been observed, apart from $^4F_{9/2} \rightarrow {}^6H_{11/2}$ (665 nm) emission transition with an excitation at 387 nm ($^6H_{15/2} \rightarrow {}^4I_{13/2}$, $^4F_{7/2}$) wavelength. Emission bands of $^1G_4 \rightarrow {}^3F_4$ (650 nm) and $^3F_3 \rightarrow {}^3H_6$ (700 nm) transitions for the Tm^{3+}:glass and glass ceramic, with excitation at $^3H_6 \rightarrow {}^1G_4$ (468 nm), have been observed. The stimulated emission cross sections of all the emission bands of Eu^{3+}, Tb^{3+}, Dy^{3+} and Tm^{3+}:glasses and glass ceramics have been computed based on their measured $\Delta\lambda$ (FWHM) and lifetimes (τ_m).

(Some figures in this article are in colour only in the electronic version)

1. Introduction

In the area of photonics, transparent crystallized glasses consisting of nonlinear optical/ferroelectric crystals have received much attention, because such materials have a high potential for applications in laser hosts, tunable waveguides, tunable fiber gratings, etc. In nonlinear optical crystals reported so far, there are many attractive TiO_2-based oxide-containing crystals, e.g. $BaTiO_3$ and $KTiOPO_4$. Adair *et al* [1] demonstrated that TiO_2 shows the highest nonlinear refractive index in a large number of optical crystals, indicating a very high oxygen hyperpolarizability of Ti–O pairs. Dimitrov and Komatsu [2] indicated that TiO_2-based glasses have large oxide ion electronic polarizabilities. Indeed, there have been some reports on crystallized glasses consisting of nonlinear optical TiO_2-based crystals [3–7]. For instance, recently, Kosaka *et al* [4] demonstrated that crystallized glasses with $Ba_3Ti_3O_6(BO_3)_2$ crystals show a strong second harmonic

[4] Author to whom any correspondence should be addressed.

intensity. It is also noted that there have been some reports on crystallized glasses consisting of GeO_2-based or-containing nonlinear optical crystals such as $LaBGeO_5$ and Bi_2GeO_5 [8–12]. Among them, it should be pointed out that transparent crystallized glass with ferroelectric $Ba_2TiGe_2O_8$ crystals in the $BaO–TiO_2–GeO_2$ system show a large second-order optical nonlinearity of $d_{33} = \sim 20$ pm V^{-1}, being comparable to the values of the $LiNbO_3$ single crystal, as reported by Takahashi *et al* [13, 14]. Very recently, Fukushima *et al* [15] reported the electronic polarizability and crystallization of $K_2O–TiO_2–GeO_2$ glasses with high TiO_2 content. It is known that the $K_2O–TiO_2–GeO_2$ system has a wide glass-forming region [16], meaning the possibility of the fabrication of glasses with a large amount of TiO_2. Since all oxides of K_2O, TiO_2 and GeO_2 have large oxide ion electronic polarizabilities [2, 17, 18], it is expected that $K_2O–TiO_2–GeO_2$ glasses would indicate high refractive indices and might have the possibility of the formation of optical nonlinear crystals through crystallization.

The Eu^{3+} ion has the lowest excited level ($^5D_0$) of the $^4f_6$ configuration which is situated below the $4f^5 5d$ configuration that shows very sharp lines extending from the visible to the near-infrared. The optical characteristics of RE ions are mainly due to electric-dipole transitions that can be affected by the local structure of the RE ion surroundings in glass. Thus, the understanding of RE ions' local structure in glasses is important, and the Eu^{3+} ion is usually used as a structure probe to find the local structure around the RE ion in glasses due to the relative simplicity of its energy level structure. The hypersensitive ratio between the integrated intensity of the induced electric-dipole $^5D_0 \rightarrow {}^7F_2$ and induced magnetic-dipole $^5D_0 \rightarrow {}^7F_1$ transitions can be used to test changes in the nature of the Eu^{3+} local surroundings and in terms of covalence and polarizability. This ratio has been also related to the odd-parity CF parameters, in such a way that the intensity of the $^5D_0 \rightarrow {}^7F_2$ transition would increase with the increase of local CF distortion around the Eu^{3+} centers [19–22]. The ground state of the Tb^{3+} ion is $^7F_6$, with its other components forming the low-lying excited states. Some of the other low-lying excited states of Tb^{3+} are $^5D_{4,3,2,1}$, $^5L_{10}$, $^5G_6$, $^5L_9$, etc. It has been found that Tb^{3+}-doped samples show very poor absorption spectra. However, they give an intense fluorescence in the green region [23, 24].

Optical properties of Dy^{3+} ions in various glasses have attracted much practical interest because its 1.3 μm emission can be utilized for optical amplification and its visible upconversion emission can be used as a solid state laser [25]. Heo and Shin have studied the absorption and mid-infrared emission spectrum of Dy^{3+} in chalcogenide glass. 1.33, 1.75, 2.9 and 4.38 μm infrared emissions were observed due to low vibrational phonon energies [26]. The emission and the laser action at the wavelengths of 2.9 and 4.4 μm from Dy^{3+} doping in different crystals and glasses have been reported by several authors [27–31]. Tannabe *et al* have studied yellow and blue luminescence of Dy^{3+} in borate glass [32]. Kumar Rai and Rai have reported the yellow upconversion emission of Dy^{3+} in tellurite glass [33]. Because of the fact that the Dy^{3+} ions show line-like and more intense absorption bands in the NIR region and interesting emission trends in the yellow wavelength region, this ion has been incorporated into these crystallized glasses, to understand the glass composition effects on the optical analysis of Dy^{3+} glasses. Among the trivalent lanthanide ions, the Tm^{3+} ion has stable excited levels suitable for emitting blue and ultraviolet upconversion fluorescence. In the last few years, the rapid expansion of bandwidth requirements for telecommunications in the 1400–1600 nm low-loss optical fiber transmission windows has generated considerable interest for Tm^{3+} ions. The $^3H_4 \rightarrow {}^3F_4$ transition at around 1470 nm allows a band extension in the spectral range corresponding to the S-band amplifier region, on the short wavelength side of the conventional erbium-doped fiber amplifier C-band at 1530–1570 nm. On the other hand, the thulium emission around 1800 nm is of interest to extend lasing capability into the 1600–1900 nm atmospheric window [34–37]. Two important factors to be satisfied in developing more efficient optical devices based on rare-earth ions are the glass host and the active ion concentration. The host matrix should have low phonon energy to minimize the multiphonon relaxation rates because the energy difference between the $^3H_4$ and the next lower-lying $^3H_5$ is not large ($\approx$4300 cm^{-1}). To avoid this problem, the glasses with low phonon energies such as fluorides, tellurites, germinates, chalcogenides and heavy-metal oxide glasses are required. It was found that the germinate glasses/glass ceramics have smaller maximum vibrational frequencies than those shown by silicate, phosphate and borate glasses [38–41]. The reduced phonon energy increases the quantum efficiency of luminescence from excited states of RE ions in these matrices, and provides the possibility to develop more efficient media for optical lasers and fiber optical amplifiers [42, 43]. In the present work we have considered these transparent $GeO_2–TiO_2–K_2O$ crystallized glasses to study the spectral properties of Eu^{3+}, Tb^{3+}, Dy^{3+} and Tm^{3+} ions.

2. Experimental studies

It is reported that large bulk glasses can be prepared in the composition of $60GeO_2–20TiO_2–20K_2O$ by using a conventional melt-quenching method and the $K_2TiGe_3O_9$ crystalline phase is formed through the crystallization [15].

Following are the Eu^{3+}-, Tb^{3+}-, Dy^{3+}- and Tm^{3+}-doped potassium–titanium–germanate glasses that are developed for the present work along with a reference glass:

$60GeO_2–20TiO_2–20K_2O$ (Host glass) (mol %)

$60GeO_2–20TiO_2–20K_2O–1.0Eu_2O_3$

$60GeO_2–20TiO_2–20K_2O–1.0Tb_4O_7$

$60GeO_2–20TiO_2–20K_2O–1.0Dy_2O_3$

$60GeO_2–20TiO_2–20K_2O–1.0Tm_2O_3$.

The starting materials used in the present work were reagent grade GeO_2, TiO_2, K_2CO_3, Eu_2O_3, Tb_4O_7, Dy_2O_3 and

Table 1. Physical properties of Eu^{3+}-, Tb^{3+}-, Dy^{3+}- and Tm^{3+}-doped glasses and their respective glass ceramics (G = glass, GC = glass ceramic).

	Data							
	Eu^{3+}		Tb^{3+}		Dy^{3+}		Tm^{3+}	
Physical quantities	G	GC	G	GC	G	GC	G	GC
Density (g cm^{-3})	3.506	3.601	3.510	3.605	3.512	3.610	3.515	3.612
Thickness, t (cm)	0.3	0.3	0.3	0.3	0.3	0.3	0.3	0.3
Refractive index, n_d (589.3)	1.717	1.772	1.719	1.779	1.722	1.783	1.726	1.787
Dielectric constant, ε	2.948	3.140	2.955	3.165	2.965	3.179	2.979	3.193
Molar volume, V_m (cm^3 mol^{-1})	28.836	28.075	29.930	29.141	28.844	28.063	28.858	28.083
Molar refractivity, R_m (cm^{-3})	11.352	11.689	11.809	12.215	11.416	11.807	11.470	11.859
Reflection loss, R (%)	6.964	7.756	6.993	7.858	7.035	7.916	7.093	7.974
Electronic polarizability, α_m (A^3)	4.502	4.635	4.683	4.844	4.527	4.682	4.549	4.703
Glass transition temperature, T_g (°C)	551	—	578	—	567	—	570	—
Glass crystallization temperature, T_c (°C)	661	—	697	—	685	—	686	—
Thermal stability, ΔT (°C) = T_c–T_g	110	—	119	—	118	—	116	—

Tm_2O_3. All weighed chemicals were powdered finely and mixed thoroughly before each batch (20 g) was melted in a platinum crucible at 1250 °C for 30 min in air. The melts were poured onto a cold brass plate and then pressed by another plate. Finally, we obtained glasses in circular designs having 2–3 cm diameter with a thickness of 0.3 cm and with a good transparency. The internal stress induced in the glasses during melt quenching is released by annealing at 400 °C for 5 h. The glasses were mechanically polished to a mirror finish with CeO_2 powder. We have prepared the Eu^{3+}-, Tb^{3+}-, Dy^{3+}- and Tm^{3+}-doped transparent glass ceramics with heat treatment at 590 °C for 3 h, as reported earlier [15]. All the glasses retain good transparency for optical measurements, even after heat treatment at 590 °C for 3 h. Densities of the base glasses and glass ceramics were determined by means of the Archimedes method using distilled water as an immersion liquid. An Abbe refractometer was used to measure the refractive indices at the Na (589.3 nm) lamp wavelength. The powder x-ray diffraction (XRD) spectrum was obtained on a Rigaku D/MAX-RA diffractometer with an Ni filter and Cu Kα (=1.542 Å) radiation with an applied voltage of 340 kV and 20 mA anode current, calibrated with Si at the rate of 2 °C min^{-1}. Differential thermal analysis (DTA) measurements were carried out on an SDT Q600 in the temperature range of 30–1000 °C, at the rate of 10 °C min^{-1}, under an N_2 gas atmosphere. The UV–vis/NIR absorption spectra were measured by a Hitachi F-4100 double beam spectrophotometer. The photoluminescence spectra were measured by a Hitachi F-4500 fluorescence spectrophotometer with 450 W Xe lamp power. The fluorescence decay curves were recorded by using a FLS920 fluorescence spectrophotometer. All the measurements were carried out at room temperature. Table 1 presents the physical properties of Eu^{3+}-, Tb^{3+}-, Dy^{3+}- and Tm^{3+}-doped glasses and their respective glass ceramics.

3. Results and discussion

Figure 1 presents the XRD profiles of the $60GeO_2$–$20TiO_2$–$20K_2O$–$1.0Eu_2O_3$ glass and transparent crystallized glass. The XRD pattern of glass exhibits the broad hump characteristic of the amorphous state. The XRD pattern of glass heat-treated at 590 °C/3 h exhibits several sharp diffractions that were assigned to the $K_2TiGe_3O_9$ crystalline phase [44, JCPDS No. 27-394]. It should be pointed out that the chemical composition of $60GeO_2$–$20TiO_2$–$60K_2O$ corresponds to the stoichiometric composition of the $K_2TiGe_3O_9$ phase. Grujic *et al* [45] also reported the formation of $K_2TiGe_3O_9$ crystals in $60GeO_2$–$20TiO_2$–$20K_2O$ glass. Figure 2 shows the DTA profiles of all the studied glasses. From these profiles, the glass transition temperature (T_g) and crystallization temperature (T_c) of Eu^{3+}-, Tb^{3+}-, Dy^{3+}- and Tm^{3+}-doped glasses have been identified and from them glass thermal stabilities were calculated and listed in table 1. T_g is related to the density of covalent cross-linking, the number and strength of the coordinate links formed between oxygen atoms and the cation, and the oxygen density of the network. Higher values of this factor correspond to higher T_g. Therefore, to clarify the change of T_g with the composition, the combined effects of the different cations must be considered. In particular, the coordination of each cation will be strongly influenced by the number of coordinate links formed by the other ones in the glass network.

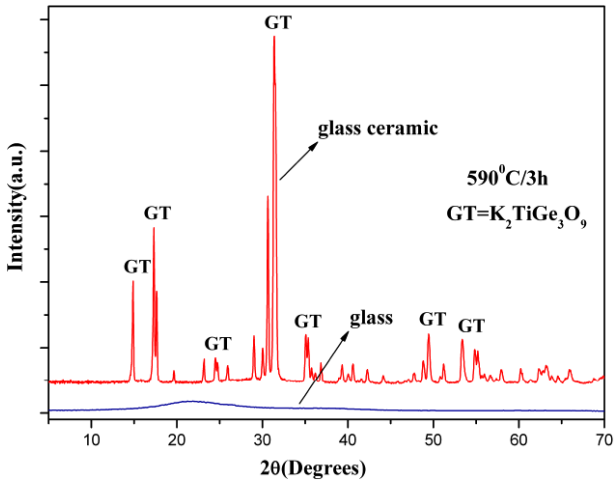

Figure 1. XRD profiles of the Eu^{3+}-doped glass and glass ceramic.

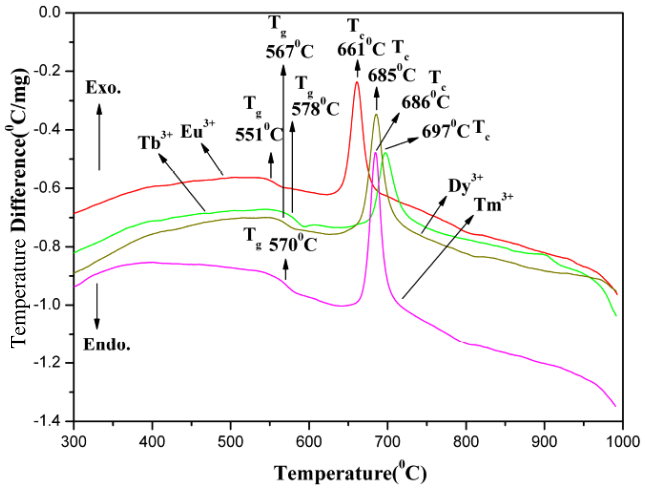

Figure 2. DTA profiles of the Eu^{3+}-, Tb^{3+}-, Dy^{3+}- and Tm^{3+}-doped glasses.

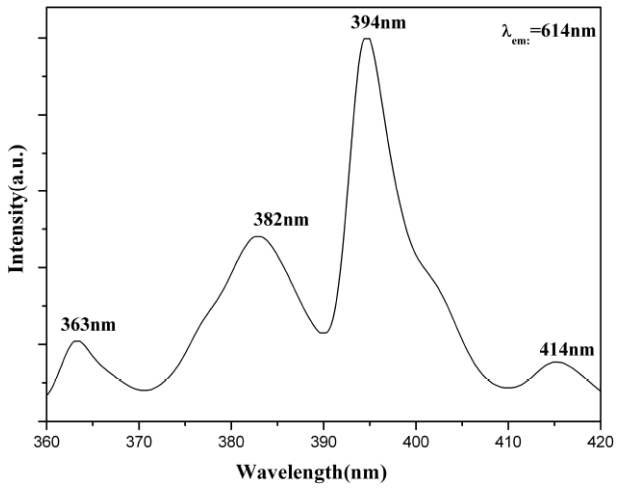

Figure 3. Excitation spectrum of 1 mol% Eu^{3+}-doped glass ceramic.

3.1. Eu^{3+}

Figure 3 shows the excitation spectrum of the 1 mol% Eu^{3+}-doped glass ceramic, monitoring emission at 614 nm. From this spectrum, four excitation bands which could be assigned to the electronic transitions of $^7F_0 \rightarrow {}^5D_4$ at 363 nm, $^7F_0 \rightarrow {}^5L_7$ at 382 nm, $^7F_0 \rightarrow {}^5L_6$ at 394 nm and $^5F_0 \rightarrow {}^5D_3$ at 414 nm are identified. Only the prominent excitation peak at 394 nm has been selected for the measurement of emission spectra of Eu^{3+}:glass and glass ceramic. Figure 4 shows emission spectra of Eu^{3+}:glass and glass ceramic, with emission bands at 578, 592, 614, 653 and 702 nm, which are assigned to the transitions from the $^5D_0$ level to the $^7F_0$, $^7F_1$, $^7F_2$, $^7F_3$ and $^7F_4$ levels, respectively [46]. The inset shows the enlarged spectra of $^7F_3$ and $^7F_4$ emission bands of glass and glass ceramic. All these observed emission bands are with higher intensity in glass ceramic compared to glass due to the $K_2TiGe_3O_9$ crystalline phase. Due to high non-radiative relaxation from excited states of energy higher than the $^5D_0$ state, the intense emission bands in the range 570–

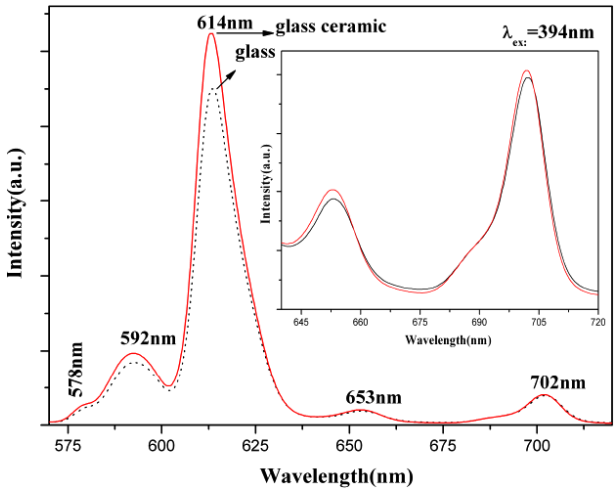

Figure 4. Emission spectra of 1 mol% Eu^{3+}-doped glass and glass ceramic. (Inset shows the enlarged spectra of $^5D_0 \rightarrow {}^7F_{3,4}$ emission bands.)

710 nm are caused by the $^5D_0 \rightarrow {}^7F_{J(=0-4)}$ transitions. The intensity of an emission transition is proportional to the radiative decay of these transitions. It is well known that the probability of the $^5D_0 \rightarrow {}^7F_2$ transition is very sensitive to the changes in the chemical surroundings of the Eu^{3+} ions. The intensity of the electric-dipole $^5D_0 \rightarrow {}^7F_2$ transition is significantly affected by the degree in the center of symmetry in the environment around the Eu^{3+} ions. Conversely, the $^5D_0 \rightarrow {}^7F_1$ emission at 592 nm is allowed by magnetic-dipole consideration. When Eu^{3+} ions are situated at low-symmetry sites, the electric-dipole transition has larger probability than the magnetic-dipole transition [47, 48]. Intra-f electrons could occur via electric-dipole, magnetic-dipole transitions, electric quadrupole, vibronic transitions and phonon-assisted energy transfer (ET) arising from ion–ion coupling, and multiphonon emissions. In glassy materials, due to the absence of a center of symmetry, mixing of the 4f orbitals with an opposite-parity orbital takes place and consequently gives rise to the existence of ED transitions [49, 50]. The absence of emissions starting from the excited levels of $^5D_{J(=1-3)}$ is due to the high energy phonons found in the glasses, i.e. when the Eu^{3+} ions are excited to any level above the $^5D_0$, there is a fast non-radiative multiphonon relaxation to this level. Thus the emissions from $^5D_{J(=1-3)}$ to ^7F_J are several orders smaller than that of $^5D_0 \rightarrow {}^7F_J$ [51]. The emission process of the Eu^{3+} ions, particularly under the excitation of the 394 nm, could be considered based on the luminescent dynamics. The ratio between $^5D_0 \rightarrow {}^7F_2$ (ED) and $^5D_0 \rightarrow {}^7F_1$ (MD) emission intensities provides valuable information about the red color richness in comparison with orange emission in developing strongly red luminescent optical systems. In our studied Eu^{3+} glass and glass ceramic, this ratio is 5.274 and 5.345, respectively. Figure 5 shows the energy level scheme of all the observed excitation and emission transitions of Eu^{3+}-doped glass/glass ceramic with 394 nm excitation. From the $^5D_0$ level the Eu^{3+} ions decay radiatively, since the large energy difference of the $^7F_6$ level presents the possibility of

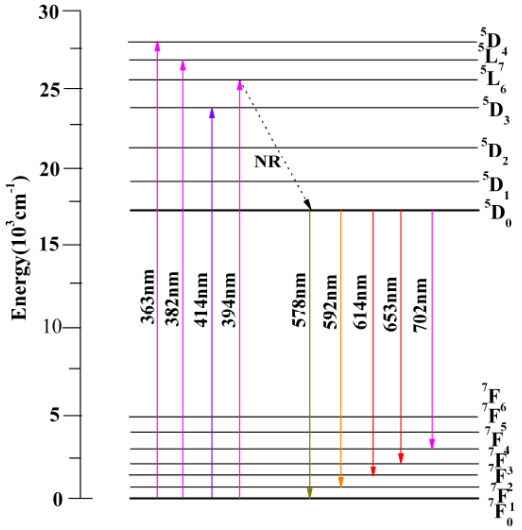

Figure 5. Energy level scheme of all the observed excitation and emission transitions of Eu^{3+}-doped glass.

multiphonon relaxation as shown in the energy level scheme. Figures 6(a) and (b) show the decay curves of the five emission transitions of ($^5D_0 \rightarrow {}^7F_{0-4}$) of the Eu^{3+} (1.0 mol%)-doped glass and glass ceramic at $\lambda_{ex:} = 394$ nm ($^7F_0 \rightarrow {}^5L_6$). The single exponential decay curves of these emission transitions indicate the non-energy transfer between Eu^{3+} ions. Compared to glass, glass ceramic emission transitions have shown longer lifetimes due to the $K_2TiGe_3O_9$ crystalline phase. The emission cross section is an important parameter and its value signifies the rate of energy extraction from the optical material. From the measured emission bands the stimulated emission cross section σ_p^E could be estimated by

$$\sigma_p^E = \frac{\lambda_p^4}{8\pi c n^2 \Delta\lambda_p \tau_m},$$

where c is the light velocity, n is the refractive index, λ_p is the emission peak wavelength, $\Delta\lambda_p$ is the width of the emission band which could be calculated by integrating the intensity of the luminescence lineshape and dividing it by the intensity at the peak wavelength and τ_m is the measured lifetime [52]. Table 2(i) presents the emission cross-section values of the Eu^{3+}-doped glass and glass ceramic. One of the most important properties of materials, which is closely related to their applicability in the field of optics and electronics, is the electronic polarizability. Estimation of the state of polarizability of the ions is the subject of the so-called polarizability approach based on the Lorentz–Lorenz equation giving the relationship between molar refraction, R_m, and refractive index, n:

$$R_m = \left[\frac{n^2-1}{n^2+2}\right]\left(\frac{M}{d}\right) = \left[\frac{n^2-1}{n^2+2}\right]V_m = 4\pi\alpha_m N/3$$

where M is the molecular weight, d is the density, V_m is the molar volume, α_m is the molar polarizability and N is Avogadro's number [53]. This equation gives the average molar refraction for isotropic substances such as liquids,

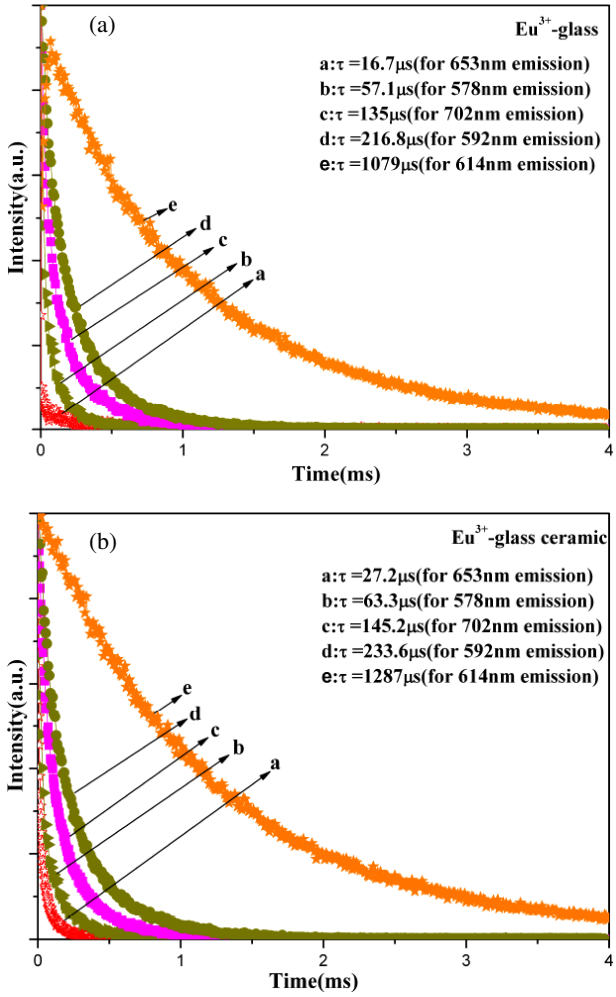

Figure 6. (a) Decay curves of the 1 mol% Eu^{3+}-doped glass. (b) Decay curves of the 1 mol% Eu^{3+}-doped glass ceramic.

glasses and cubic crystals. The values of molar refractivity and electronic polarizability of the Eu^{3+}-, Tb^{3+}-, Dy^{3+}- and Tm^{3+}-doped glasses and glass ceramics are summarized in table 1. All these values in nanocrystallized glasses are larger than those in the glasses. These data indicate that nanocrystals have a larger electron donor ability compared with the base glass. This means that the electron state in nanocrystals is more floppy. The refractive index of the Eu^{3+}, Tb^{3+}, Dy^{3+} and Tm^{3+} glass ceramics, polished mechanically by using CeO_2 powders, was higher than the corresponding glasses as shown in table 1. It is obvious that the increase in refractive index is due to the $K_2TiGe_3O_9$ crystalline phase itself present in the glasses. Indeed, the presence of the $K_2TiGe_3O_9$ phase only was confirmed in the polished crystallized glass from the XRD pattern (figure 1).

3.2. Tb^{3+}

Figure 7 shows the excitation spectrum of 1 mol% Tb^{3+}-doped glass ceramic, monitoring emission at 549 nm. Only a prominent excitation peak at 378 nm ($^7F_6 \rightarrow {}^5G_6$) has been identified from this spectrum. Figure 8 shows the emission spectra of Tb^{3+}-doped glass and glass ceramic. All these

Table 2. Emission peak wavelengths (λ_p), full widths at half-maximum (FWHM, $\Delta\lambda_p$), measured lifetimes (τ_m) and stimulated emission cross sections (σ^E) of different (i) Eu^{3+} (ii) Tb^{3+} (iii) Dy^{3+} and (iv) Tm^{3+} emission transitions (G = glass, GC = glass ceramic).

Emission transitions	λ_p (nm)	$\Delta\lambda_p$ (nm)	τ_m (μs)	$\sigma^E(\times10^{20})$ cm^2
(i) Eu^{3+}:glass and glass ceramics measured with 394 nm excitation wavelength				
$^5D_0 \rightarrow {}^7F_0$	578	4	57.1	22.00 (G)
		5	63.3	14.91 (GC)
$^5D_0 \rightarrow {}^7F_1$	592	11	216.8	2.319 (G)
		14	233.6	1.587 (GC)
$^5D_0 \rightarrow {}^7F_2$	614	12	1079	0.4942 (G)
		13	1287	0.3591 (GC)
$^5D_0 \rightarrow {}^7F_3$	653	10	16.7	49.02 (G)
		11	27.2	25.69 (GC)
$^5D_0 \rightarrow {}^7F_4$	702	13	135	6.230 (G)
		13	145.2	5.438 (GC)
(ii) Tb^{3+}:glass and glass ceramics measured with 378 nm excitation wavelength				
$^5D_4 \rightarrow {}^7F_6$	490	20	490.6	0.2639 (G)
		20	612.1	0.1975 (GC)
$^5D_4 \rightarrow {}^7F_5$	549	14	773	0.3770 (G)
		15	857.4	0.2962 (GC)
$^5D_4 \rightarrow {}^7F_4$	586	17	148.1	2.104 (G)
		18	218.6	1.257 (GC)
$^5D_4 \rightarrow {}^7F_3$	621	15	135.3	3.291 (G)
		16	193.4	2.015 (GC)
(iii) Dy^{3+}:glass and glass ceramics measured with 387 nm excitation wavelength				
$^4F_{9/2} \rightarrow {}^6H_{15/2}$	485	17	59.3	2.457 (G)
		18	81.9	1.567 (GC)
$^4F_{9/2} \rightarrow {}^6H_{13/2}$	576	16	144	2.138 (G)
		16	167.9	1.711 (GC)
$^4F_{9/2} \rightarrow {}^6H_{11/2}$	665	14	36.1	0.1732 (G)
		15	59.8	0.091 02 (G)
(iv) Tm^{3+}:glass and glass ceramics measured with 468 nm excitation wavelength				
$^1G_4 \rightarrow {}^3F_4$	650	7	1.8	631.2 (G)
		9	3.6	229.0 (GC)
$^3F_3 \rightarrow {}^3H_6$	707	8	1.6	835.7 (G)
		8	27.2	45.9 (GC)

observed emission bands are with higher intensity in glass ceramic compared to glass due to the $K_2TiGe_3O_9$ crystalline phase. The emission transitions have shown sharp emission bands due to the f–f inner shell transitions, from the excited level to the lower level such as $^5D_4 \rightarrow {}^7F_{J(=0-6)}$ for Tb^{3+}. When Tb^{3+} ions are excited by UV radiation, electronic transitions of either $^5D_3 \rightarrow {}^7F_J$ (blue emission) or successive $^5D_3 \rightarrow {}^5D_4$ and $^5D_4 \rightarrow {}^7F_J$ (green emission) take place, where $J = 0, 1, \ldots, 6$ [54]. Bands with smaller widths and larger intensities are noticed from 480 to 630 nm. From the emission spectrum, transitions such as $^5D_4 \rightarrow {}^7F_6$ (490 nm), $^5D_4 \rightarrow {}^7F_5$ (549 nm), $^5D_4 \rightarrow {}^7F_4$ (586 nm) and $^5D_4 \rightarrow {}^7F_3$ (621 nm) have been identified [55]. The intense green emission is at 543 nm and arises from the Laporte-forbidden $^5D_4 \rightarrow {}^7F_5$ transition [56]. The transition $^5D_4 \rightarrow {}^7F_6$ obeys the magnetic-dipole selection rule of $\Delta J = \pm1$ [57]. Figure 9 shows the energy level scheme of all the observed excitation and emission transitions of Tb^{3+}-doped glass and glass ceramic. From $^5D_4$ level the Tb^{3+} ions decay radiatively, since the large energy difference of the $^7F_0$ level presents the possibility of multiphonon relaxation as shown in the energy level scheme. Figures 10(a) and (b) show the decay curves of the observed four emission transitions of Tb^{3+}-doped glass and glass ceramic which are in single exponential. Table 2(ii) presents the emission cross-section values of the Tb^{3+}-doped glass and glass ceramic.

3.3. Dy^{3+}

Figure 11 shows the absorption spectrum of 1 mol% Dy^{3+}-doped glass ceramic. The bands are assigned from the ground state, $^6H_{15/2}$. The transitions from the next excited state $^6H_{13/2}$ may be ruled out due to thermalization as the energy gap between $^6H_{15/2}$ and $^6H_{13/2}$ is around 3000 cm^{-1}. From this spectrum, the levels of $^4I_{15/2}$ (454 nm), $^6F_{3/2}$ (746 nm), $^6F_{5/2}$ (795 nm), $^6F_{7/2}$ (893 nm), ($^6H_{7/2}$, $^6F_{9/2}$) (1082 nm), ($^6F_{11/2}$, $^6H_{9/2}$) (1260 nm) and $^6H_{11/2}$ (1648 nm) are well resolved [46]. The position and intensity of certain transitions of rare-earth ions are found to be very sensitive to the environment around the ion. Such transitions are termed hypersensitive transitions [58]. All known hypersensitive transitions obey the selection rule $|\Delta S| = 0$, $|\Delta L| \leqslant 2$, $|\Delta J| \leqslant 2$ [58]. In the case of the Dy^{3+} ($4f^9$) ion, the

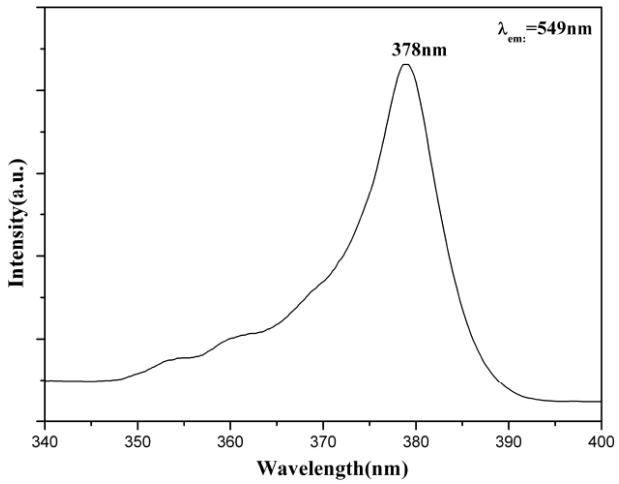

Figure 7. Excitation spectrum of 1 mol% Tb^{3+}-doped glass ceramic.

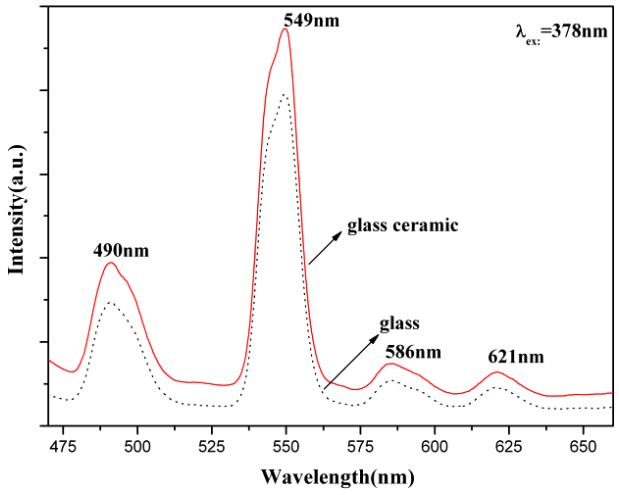

Figure 8. Emission spectra of 1 mol% Tb^{3+}-doped glass and glass ceramic.

hypersensitive transition ($^6F_{11/2}$, $^6H_{9/2}$) is found to be more intense than the other transitions. Figure 12 shows the excitation spectrum of 1 mol% Dy^{3+}-doped glass ceramic, monitoring emission at 576 nm. We have observed several excitation bands from this excitation spectrum and these are assigned to the electronic transitions with the ground level $^6H_{15/2}$ to higher energy levels of Dy^{3+}, i.e. $^6H_{15/2} \rightarrow {}^4M_{15/2} + {}^6P_{7/2}$ (353 nm), $^6H_{15/2} \rightarrow {}^4I_{11/2}$ (366 nm), $^6H_{15/2} \rightarrow {}^4I_{13/2} + {}^4F_{7/2}$ (387 nm), $^6H_{15/2} \rightarrow {}^4G_{11/2}$ (425 nm), $^6H_{15/2} \rightarrow {}^4I_{15/2}$ (454 nm) and $^6H_{15/2} \rightarrow {}^4F_{9/2}$ (471 nm) based on the energy levels reported earlier [46]. From these excitation transitions, only a prominent transition (387 nm) has been selected for the measurement of emission spectra of Dy^{3+}:glass and glass ceramic. Figure 13 presents the emission spectra of 1 mol% Dy^{3+}-doped glass and glass ceramic with 387 nm excitation wavelength. When the $^4I_{13/2} + {}^4F_{7/2}$ level of Dy^{3+} is excited with 387 nm wavelength, though this level is within the thermal excitation energy at room temperature, we do not get any fluorescence from this level. The Dy^{3+} ions will depopulate non-radiatively from the $^4I_{13/2} + {}^4F_{7/2}$ level to

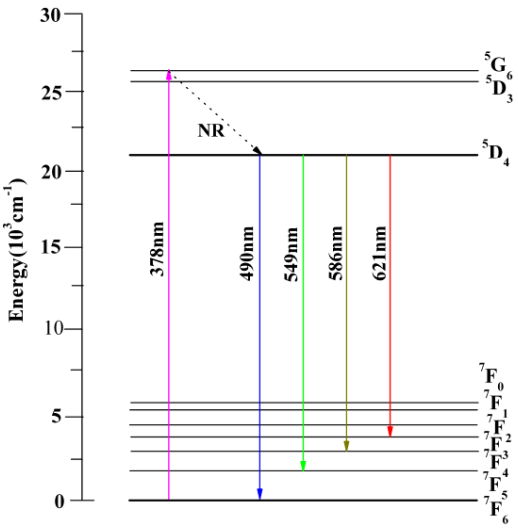

Figure 9. Energy level scheme of all the observed excitation and emission transitions of Tb^{3+}-doped glass.

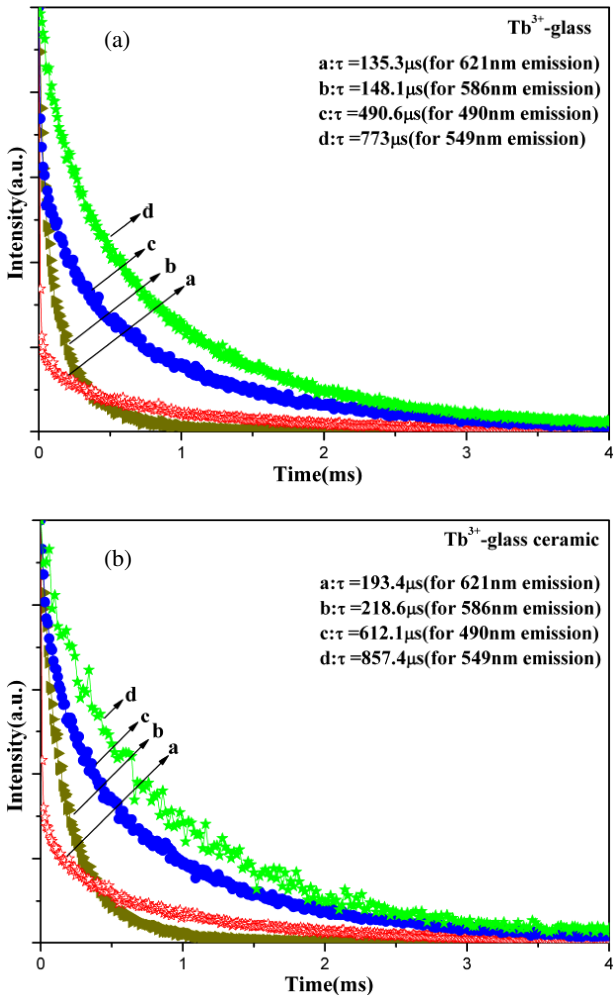

Figure 10. (a) Decay curves of the 1 mol% Tb^{3+}-doped glass. (b) Decay curves of the 1 mol% Tb^{3+}-doped glass ceramic.

the stable eigenstate of Dy^{3+}, $^4F_{9/2}$ whose energy from the ground state is ∼20 660 cm^{-1}. This state is separated from the next lower-lying level ($^6F_{1/2}$) by about 6000 cm^{-1}, which

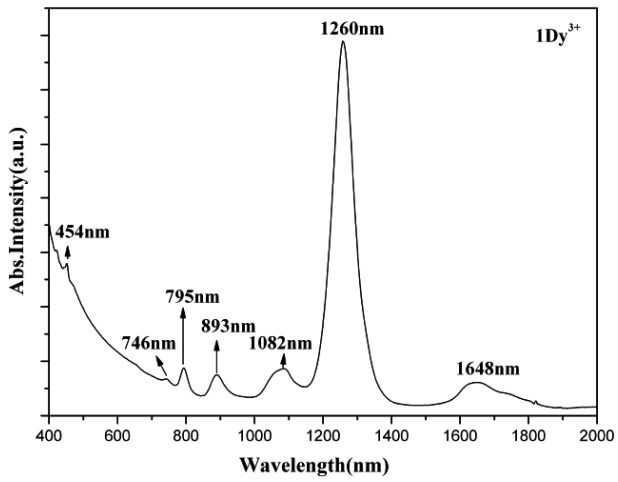

Figure 11. Absorption spectrum of 1 mol% Dy^{3+}-doped glass ceramic.

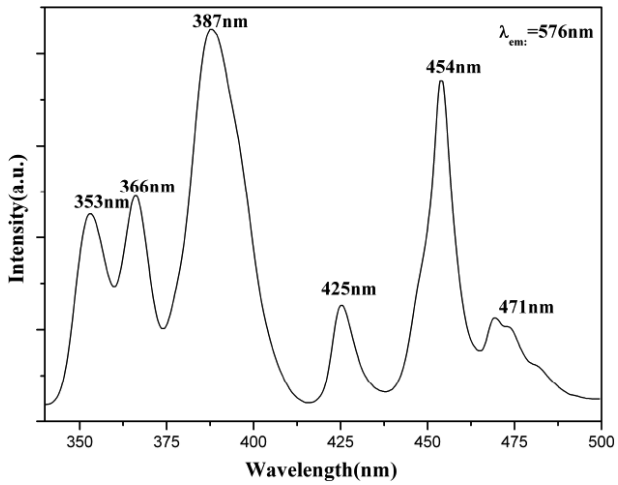

Figure 12. Excitation spectrum of 1 mol% Dy^{3+}-doped glass ceramic.

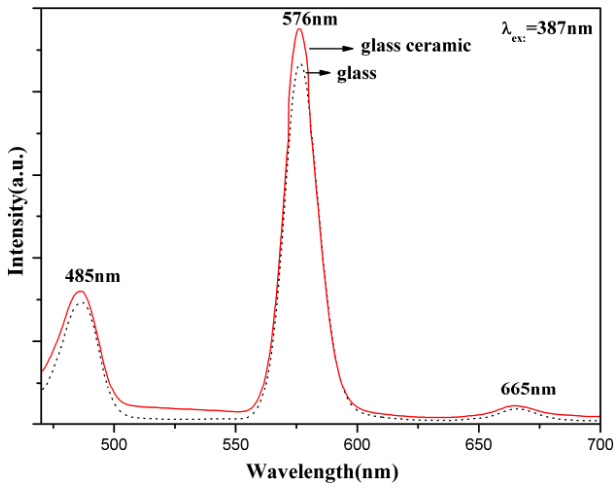

Figure 13. Emission spectra of 1 mol% Dy^{3+}-doped glass and glass ceramic.

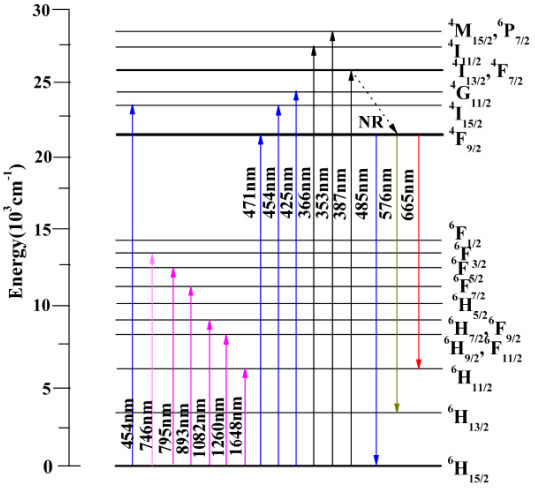

Figure 14. Energy level scheme of all the observed absorption, excitation and emission transitions of Dy^{3+}-doped glass.

makes the multiphonon relaxation negligible in spite of high phonon energies of the host (∼900 cm^{-1}). It appears that only radiative transitions and relaxation by non-radiative energy transfer processes could be depopulating the $^4F_{9/2}$ state [59]. From these emission spectra, we have observed two emission bands centered at 485 and 576 nm, which could be assigned to $^4F_{9/2} \rightarrow {}^6H_{15/2}$ and $^4F_{9/2} \rightarrow {}^6H_{13/2}$ transitions, from Dy^{3+}-doped glass and glass ceramic apart from a week emission band at $^4F_{9/2} \rightarrow {}^6H_{11/2}$ (665 nm). Among these, the transition $^6F_{9/2} \rightarrow {}^6H_{13/2}$ has shown a bright yellow emission intensity, i.e. a major part of the emission intensity is contained in the $^4F_{9/2} \rightarrow {}^6H_{13/2}$ transition. Dy^{3+}-doped glass ceramic has shown stronger emissions compared to Dy^{3+}-doped glass due to the $K_2TiGe_3O_9$ crystalline phase present in it. The Dy^{3+}-doped glass ceramic showed a bright yellow emission under a UV source also. Figure 14 presents the energy level scheme of all the observed absorption, excitation and emission transitions of Dy^{3+}-doped glass and glass ceramic. We have measured the lifetimes of blue (485 nm), yellow (576 nm) and red (665 nm) emission transitions with excitation wavelength at 387 nm for Dy^{3+}-doped glass and glass ceramic, and presented them in figures 15(a) and (b). From these decay curves, we observed that, compared to glass, glass ceramic has shown longer lifetimes for the observed emission transitions. It confirms a fact that long-range crystalline ordering may be crucial for the effects observed because the site coordination of the Dy^{3+} ions is so strongly defined. Table 2(iii) presents the emission cross-section values of the Dy^{3+}-doped glass and glass ceramic.

3.4. Tm^{3+}

Figure 16 shows the absorption spectrum of 1 mol% Tm^{3+}-doped glass ceramic. The rare-earth ions are characterized by a partially filled 4f shell which is shielded by $5s^2$ and $5p^6$ electrons. All transitions in the absorption spectrum of Tm^{3+} start from the ground state $^3H_6$ to the various excited states. The transitions observed in the absorption spectrum of Tm^{3+} are intra-configurational (f–f) transitions with almost the absence of overlap with the surrounding ions. The spectrum

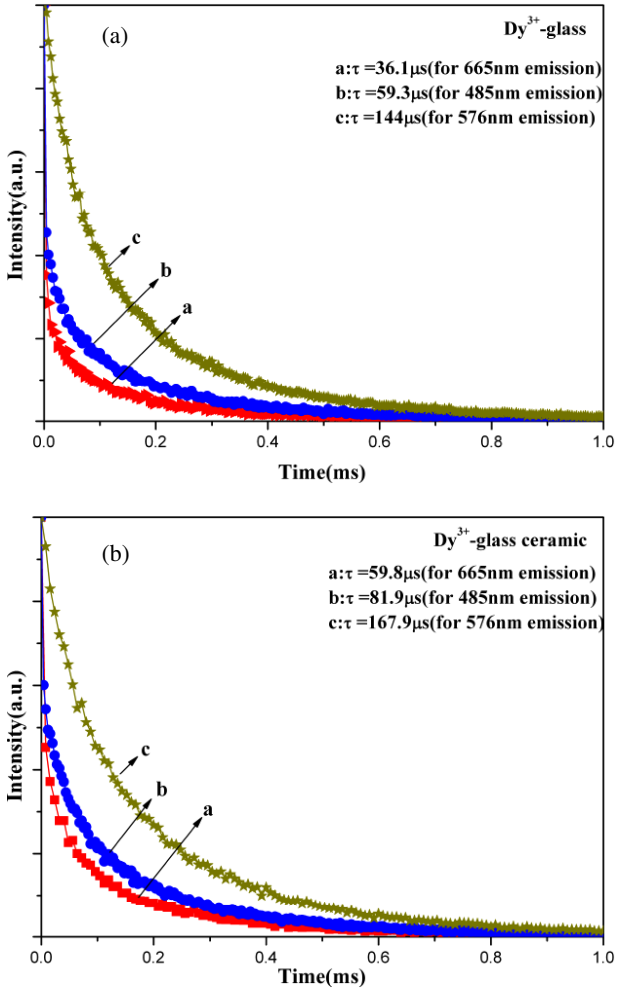

Figure 15. (a) Decay curves of the 1 mol% Dy^{3+}-doped glass. (b) Decay curves of the 1 mol% Dy^{3+}-doped glass ceramic.

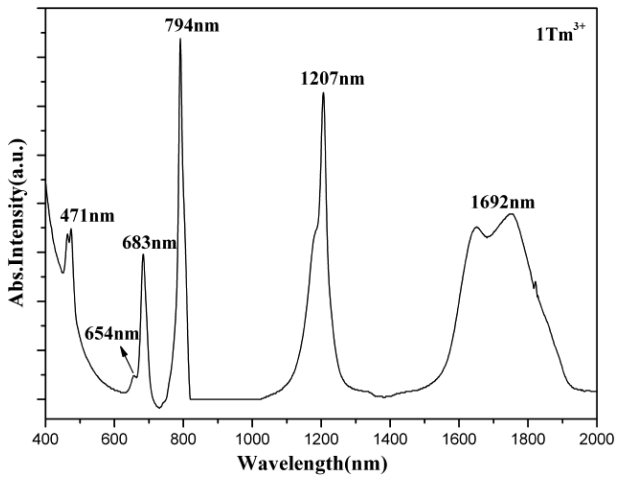

Figure 16. Absorption spectrum of 1 mol% Tm^{3+}-doped glass ceramic.

is characterized by six bands corresponding to the transitions starting from the $^3H_6$ ground state to the different higher levels $^1G_4$ (471 nm), $^3F_2$ (654 nm), $^3F_3$ (683 nm), $^3H_4$ (794 nm), $^3H_5$ (1207 nm) and $^3F_4$ (1692 nm) [46]. The absorption bands measured are all dominated by electric-dipole transitions except the transition $^3H_6 \rightarrow {}^3H_5$, which contains electric-dipole and magnetic-dipole contributions. Figure 17 presents the excitation spectrum of 1 mol% Tm^{3+}-doped glass ceramic, monitoring emission at 700 nm. A broad excitation band centered at 468 nm ($^3H_6 \rightarrow {}^1G_4$) is observed from this spectrum. Figure 18 shows the emission spectra of 1 mol% Tm^{3+}-doped glass and glass ceramic with 468 nm excitation. From these spectra, emission bands centered at 650 nm ($^1G_4 \rightarrow {}^3F_4$) and 700 nm ($^3F_3 \rightarrow {}^3H_6$) are observed for the 1 mol% Tm^{3+}-doped glass and glass ceramic, respectively. Of them, $^3F_3 \rightarrow {}^3H_6$ (700 nm) has shown bright emission intensity. Tm^{3+}-doped glass ceramic has shown stronger emissions compared to Tm^{3+}-doped glass due to the $K_2TiGe_3O_9$ crystalline phase present in it. Figure 19 presents the energy level scheme of all observed absorption, excitation and emission transitions of Tm^{3+}-doped glass/glass ceramic. We have measured the lifetimes of the observed

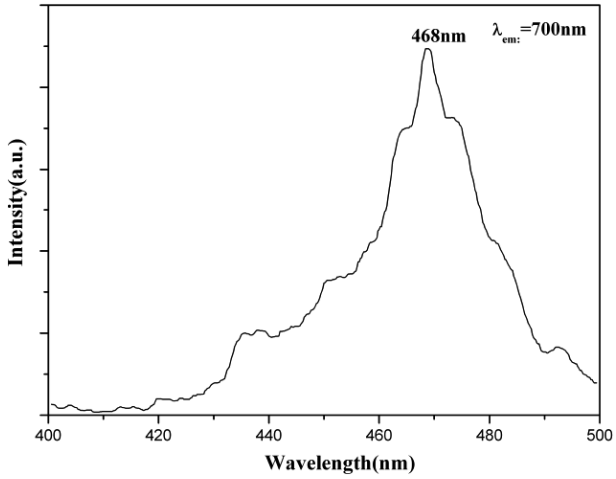

Figure 17. Excitation spectrum of 1 mol% Tm^{3+}-doped glass ceramic.

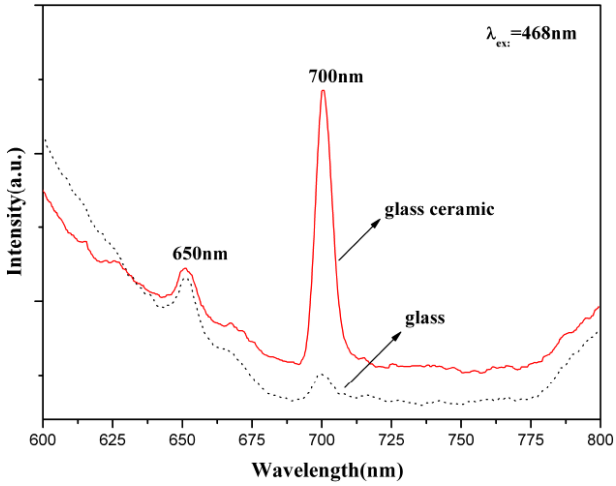

Figure 18. Emission spectra of 1 mol% Tm^{3+}-doped glass and glass ceramic.

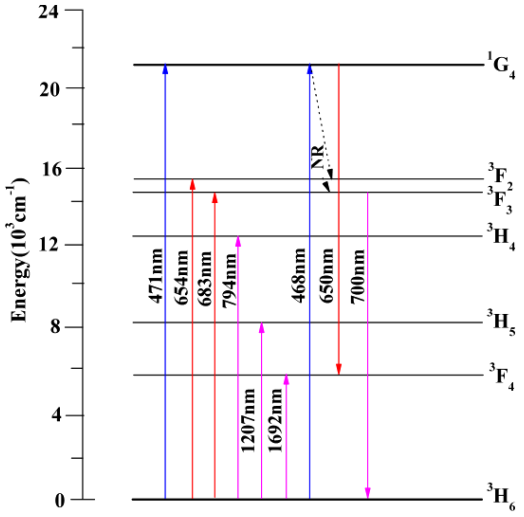

Figure 19. Energy level scheme of all observed absorption, excitation and emission transitions of Tm^{3+}-doped glass.

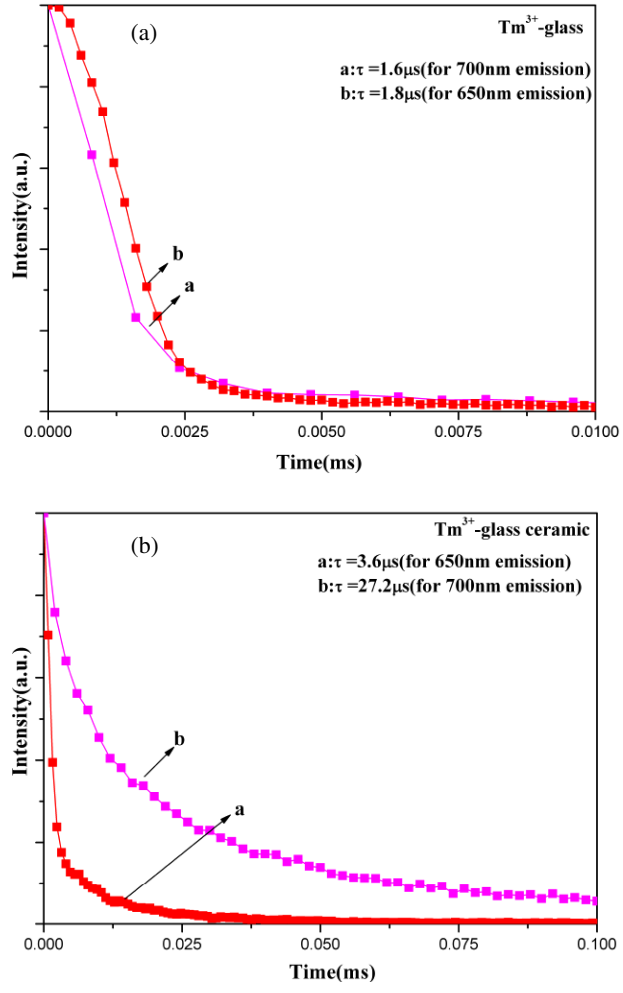

Figure 20. (a) Decay curves of the 1 mol% Tm^{3+}-doped glass. (b) Decay curves of the 1 mol% Tm^{3+}-doped glass ceramic.

emission transitions with the excitation wavelength (468 nm), and figures 20(a) and (b) present the decay curves of these two emission transitions of Tm^{3+} glass and glass ceramic, respectively. From these decay curves, we observed that, compared to glass, glass ceramic has shown longer lifetimes for the observed emission transitions. Table 2(iv) presents the emission cross-section values of the Tm^{3+}-doped glass and glass ceramic.

4. Conclusions

In summary, it is concluded that we have successfully developed transparent $K_2TiGe_3O_9$ crystallized glasses with Eu^{3+}, Tb^{3+}, Dy^{3+} and Tm^{3+} as dopant ions for their optical characterization. For Eu^{3+}-doped glass and glass ceramics, five emission bands centered at 578 nm ($^5D_0 \rightarrow {}^7F_0$), 592 nm ($^5D_0 \rightarrow {}^7F_1$), 614 nm ($^5D_0 \rightarrow {}^7F_2$), 653 nm ($^5D_0 \rightarrow {}^7F_3$) and 702 nm ($^5D_0 \rightarrow {}^7F_4$) have been observed with 394 nm ($^5D_0 \rightarrow {}^7L_6$) excitation wavelength. Of them, 614 nm ($^5D_0 \rightarrow {}^7F_2$) has shown bright reddish-orange emission. For Tb^{3+}-doped glass and glass ceramic, four emission bands centered at 490 nm ($^5D_4 \rightarrow {}^7F_6$), 549 nm ($^5D_4 \rightarrow {}^7F_5$), 586 nm ($^5D_4 \rightarrow {}^7F_4$) and 621 nm ($^5D_4 \rightarrow {}^7F_3$) have been observed with an excitation at 378 nm ($^3F_6 \rightarrow {}^5G_6$) wavelength. Of them, 549 nm ($^5D_4 \rightarrow {}^7F_5$) has shown bright green emission. With regard to Dy^{3+}:glass and glass ceramic, a blue emission band centered at 485 nm ($^4F_{9/2} \rightarrow {}^6H_{15/2}$) and a bright fluorescent yellow emission at 576 nm ($^4F_{9/2} \rightarrow {}^6H_{13/2}$) have been observed, apart from $^4F_{9/2} \rightarrow {}^6H_{11/2}$ (665 nm) emission transition with an excitation at 387 nm ($^6H_{15/2} \rightarrow {}^4I_{13/2}$, $^4F_{7/2}$) wavelength. Emission bands of $^1G_4 \rightarrow {}^3F_4$ (650 nm) and $^3F_3 \rightarrow {}^3H_6$ (700 nm) transitions for the Tm^{3+}:glass and glass ceramic, with excitation at $^3H_6 \rightarrow {}^1G_4$ (468 nm), have been observed. Upon exposure to the UV rays, Eu^{3+}, Tb^{3+} and Dy^{3+} glasses/glass ceramics have shown bright red, green and yellow emissions, respectively, from their surfaces. We have measured the decay curves and also evaluated stimulated emission cross sections of these emission bands of Eu^{3+}, Tb^{3+}, Dy^{3+} and Tm^{3+} glasses. Based on the results given in tables 1 and 2 and different figures (figures 1–20), these could be suggested as potential and interesting optical luminescent materials of technological importance. The crystallization plays an important role in the observed enhanced emission properties; particularly in the IR oscillators, their width and spectral shift is very important. This reflects a fact of fixed position of the rare-earth ions for the crystalline states with respect to the glass-like states.

Acknowledgments

This work was financially supported by the National Nature Science Foundation of China (grant nos. 50672087 and 60778039), the National Basic Research Program of China (2006CB806007) and the National High Technology Program of China (2006AA03Z304). This work was also supported by the program for Changjiang Scholars and Innovative Research Team in University (IRT0651).

References

[1] Adair R, Chase L L and Payne A A 1989 *Phys. Rev.* B **39** 3337
[2] Dimitrov V and Komatsu T 2005 *J. Solid State Chem.* **178** 831

[3] Bhargava A, Shelby J E and Snyder R L 1998 *J. Non-Cryst. Solids* **102** 136
[4] Kosaka S, Benino Y, Fujiwara T, Dimitrov V and Komatsu T 2005 *J. Solid State Chem.* **178** 2067
[5] Feitosa C A C, Mastelaro V R, Zanatta A R, Hernandes A C and Zanotto E D 2006 *Opt. Mater.* **28** 935
[6] Cabral A A, Fokin V M, Zanotto E D and Chinaglia C R 2003 *J. Non-Cryst. Solids* **330** 174
[7] Takahashi Y, Kitamura K, Benino Y, Fujiwara T and Komatsu T 2005 *Appl. Phys. Lett.* **86** 091110
[8] Sigaev V N, Stefanovich Yu S, Sarkisov P D and Lopatina E V 1994 *Glass Phys. Chem.* **20** 398
[9] Takahashi Y, Benino Y, Fujiwara T and Komatsu T 2001 *J. Appl. Phys.* **89** 5282
[10] Takahashi Y, Iwasaki A, Benino Y, Fujiwara T and Komatsu T 2002 *Japan. J. Appl. Phys.* **41** 3771
[11] Gupta P, Jain H, Williams D B, Kanert O and Kuechler R 2004 *J. Non-Cryst. Solids* **349** 291
[12] Pengpat K and Holland D 2003 *J. Eur. Ceram. Soc.* **23** 1599
[13] Takahashi Y, Benino Y, Fujiwara T and Komatsu T 2002 *Appl. Phys. Lett.* **81** 223
[14] Takahashi Y, Benino Y, Fujiwara T and Komatsu T 2004 *J. Appl. Phys.* **95** 3503
[15] Fukushima T, Benino Y, Fujiwara T, Dimitrov V and Komatsu T 2006 *J. Solid State Chem.* **179** 3949
[16] Imaoka M and Yamazaki T 1964 *J. Ceram. Soc. Japan* **72** 182
[17] Dimitrov V and Sakka S 1996 *J. Appl. Phys.* **79** 1736
[18] Dimitrov V and Komatsu T 1999 *J. Ceram. Soc. Japan* **107** 879
[19] Tang G, Zhu J, Zhu Y and Bai C 2008 *J. Alloys Compounds* **453** 487
[20] Bezerra M F O, Couto dos Santos M A, Monteil A and Chaussedent S 2008 *Opt. Mater.* **30** 1013
[21] Liang H, Hanzawa H, Horikawa T and Machida K I 2008 *J. Alloys Compounds* **457** L6–8
[22] Wada N and Kojima K 2007 *J. Lumin.* **126** 53
[23] Kam C H and Buddhudu S 2003 *Physica* B **337** 237
[24] Silversmith A J, Boye D M, Brewer K S, Gillespie C E, Lu Y and Campbell D L 2006 *J. Lumin.* **121** 14
[25] Duan Z, Zhang J and Hu L 2007 *J. Appl. Phys.* **101** 043110
[26] Heo J and Shin Y B 1996 *J. Non-Cryst. Solids* **196** 162
[27] Johnson L F and Guggenhiem H J 1973 *Appl. Phys. Lett.* **23** 96
[28] Barnes N P and Allen R E 1991 *IEEE J. Quantum Electron.* **27** 277
[29] Wei K, Machewirth D P, Wenzel J, Snitzer E and Sigel G H Jr 1994 *Opt. Lett.* **19** 904
[30] Tanabe S, Hanada T, Watanabe M, Hayashi T and Soga N 1995 *J. Am. Ceram. Soc.* **78** 2917
[31] Schweizer T, Hewak D W, Samson B N and Payne D N 1996 *Opt. Lett.* **21** 1594
[32] Tannabe S, Kang J, Hanada T and Soga N 1998 *J. Non-Cryst. Solids* **239** 170
[33] Kumar Rai V and Rai S B 2004 *Solid State Commun.* **132** 647
[34] Allain J Y, Monerie M and Poignant H 1989 *Electron. Lett.* **25** 1660
[35] Tanabe S, Feng X and Hanada T 2000 *Opt. Lett.* **25** 817
[36] Wu J, Yao Z, Zong J and Jiang S 2007 *Opt. Lett.* **32** 638
[37] Balda R, Fernández J, García-Revilla S and Fernández-Navarro J M 2007 *Opt. Express* **15** 6750
[38] Balda R, Fernández J, de Pablos A and Fdez-Navarro J M 1999 *J. Phys.: Condens. Matter* **11** 7411
[39] Pan Z, Morgan S H, Loper A, King V, Long B H and Collins W E 1995 *J. Appl. Phys.* **77** 4688
[40] Wachtler M, Speghini A, Pigorini S, Rolli R and Bettinelli M 1997 *J. Non-Cryst. Solids* **217** 111
[41] Ribeiro S J L, Dexpert-Ghys J, Piriou B and Mastelaro V R 1993 *J. Non-Cryst. Solids* **159** 213
[42] Canale J E, Condrate R A, Nassau K Sr and Cornilsen B C 1986 *J. Can. Ceram. Soc.* **55** 50
[43] Wang J, Lincoln J R, Brocklesby W S, Deol R S, Mackechnie C J, Pearson A, Tropper A C, Hanna D C and Payne D N 1993 *J. Appl. Phys.* **73** 8066
[44] Choisnet J, Deschanvres A and Raveau E T B 1973 *J. Solid State Chem.* **7** 408
[45] Grujic S, Blagojevic N, Tosic M, Zivanavic V and Bozovic B 2006 *J. Therm. Anal. Cal.* **83** 463
[46] Carnall W T, Fields P R and Rajnak K 1968 *J. Chem. Phys.* **49** 4452
[47] Fan X, Wu X, Wang M, Qiu J and Kawamoto Y 2004 *Mater. Lett.* **58** 2217
[48] Wang J, Song H, Kong X, Peng H, Sun B, Chen B, Zhang J, Xu W and Xia H 2003 *J. Appl. Phys.* **93** 1482
[49] Lavin U, Rodriguez-Mendoza U R, Martin I R and Rodriguez V D 2003 *J. Non-Cryst. Solids* **319** 200
[50] Jubera V, Chaminade J P, Garcia A, Guillen F and Fouassier C 2003 *J. Lumin.* **101** 1
[51] Kam C H and Buddhudu S 2004 *Physica* B **344** 182
[52] Karthikeyan B, Mohan S and Baesso M L 2003 *Physica* B **337** 249
[53] Torres F, Narita K, Benino Y, Fujiwara T and Komatsu T 2003 *J. Appl. Phys.* **94** 5265
[54] Hayakawa T, Kamata N and Yamada K 1996 *J. Lumin.* **68** 179
[55] Zhang X, Zhang J, Liang L and Su Q 2005 *Mater. Res. Bull.* **40** 281
[56] Xu Z, Li Y, Liu Z and Wang D 2005 *J. Alloys Compounds* **391** 202
[57] Hussain N S, Reddy Y P and Buddhudu S 2001 *Mater. Lett.* **48** 303
[58] Jorgensen C K and Judd B R 1964 *Mol. Phys.* **8** 281
[59] Mahato K K, Rai A and Rai S B 2005 *Spectrochim. Acta* A **61** 431